

Nanoscale atomic waveguides with suspended carbon nanotubes

V. Peano¹, M. Thorwart¹, A. Kasper², R. Egger¹

¹ Institut für Theoretische Physik, Heinrich-Heine-Universität Düsseldorf, D-40225 Düsseldorf, Germany

² NTT Basic Research Laboratories, NTT Corporation, Kanagawa 243-0198, Japan

Received: / Revised version:

Abstract We propose an experimentally viable setup for the realization of one-dimensional ultracold atom gases in a nanoscale magnetic waveguide formed by single doubly-clamped suspended carbon nanotubes. We show that all common decoherence and atom loss mechanisms are small guaranteeing a stable operation of the trap. Since the extremely large current densities in carbon nanotubes are spatially homogeneous, our proposed architecture allows to overcome the problem of fragmentation of the atom cloud. Adding a second nanowire allows to create a double-well potential with a moderate tunneling barrier which is desired for tunneling and interference experiments with the advantage of tunneling distances being in the nanometer regime.

1 Introduction

The ongoing progress in the fabrication and manipulation of micro- or nanoscale structures has recently allowed for systematic studies of ultracold atom gases, where current-carrying wires and additional magnetic bias fields generate magnetic fields trapping neutral atoms ('atom chips') [1,2]. For instance, the Bose-Einstein condensation (BEC) of microchip-confined atoms has been successfully demonstrated by several groups [3]. So far, decoherence and atom loss constitute central impediments, since atoms are relatively close to 'hot' macroscopic surfaces or current-carrying wires (with typical diameters of several μm), where the Casimir-Polder potential and Johnson noise can seriously affect stability [4,5,6]. To reduce these effects, further miniaturization to the nanoscale regime would be desirable. In particular, this is promising in the context of integrated atomic matter-wave interferometry and optics [7], and combines the strengths of nanotechnology and atomic physics. While at first sight this goal conflicts with the requirement of large currents forming tight trapping potentials, we propose that when using suspended carbon nanotubes

(NTs) [8] (with diameters of a few nm) as wires, nanoscale atom chip devices with large current densities can be designed. In turn, these devices allow to trap ultracold atom gases basically free of trap-induced decoherence or atom losses, with the gas containing few tens of atoms. Since disorder is generally weak in NTs, the (extremely large) current density distribution is spatially homogeneous, which allows to overcome the problem of fragmentation of the atom cloud which plagues common atom chip designs. Moreover, they can be built with state-of-the-art technology.

With relevant length scales below optical and cold-atom de Broglie wavelengths, this also paves the way for the observation of interesting and largely unexplored many-body physics in one dimension (1D) [9]. Examples include the interference properties of interacting matter waves [10], the 1D analogue of the BEC-BCS crossover [11] and shape resonances in 1D trapping potentials [12]. Previous realizations of 1D cold atoms were reported using optical lattices [13,14,15] and magnetic traps [16], but they involve arrays of 1D or elongated 3D systems, where it is difficult to separately manipulate a single 1D atom cloud (the distances between the 1D systems composing the array are few hundred nm). A noteworthy advantage of our proposal against dipole optical trap is that arrays of many NT waveguides can be built, where it is possible to manipulate an individual trap by changing the current through an individual NT. A further advantage of our proposal against the common macroscopic atom chips is that it minimizes unwanted substrate effects and implies a drastically reduced transverse size (a few nm) of the cloud.

2 The setup

A typical proposed nanoscale waveguide setup to confine ultracold atoms to 1D is sketched in Fig. 1. The setup employs a single suspended doubly-clamped NT (left NT in Fig. 1, the second suspended NT on the

right will be used to create a double-well potential, see below), where nanofabrication techniques routinely allow for trenches with typical depths and lengths of several μm [8]. To minimize decoherence and loss effects [5], the substrate should be insulating apart from thin metal strips to electrically contact the NTs. Since strong currents (hundreds of μA) are necessary, thick multiwall nanotubes (MWNTs) or ‘ropes’ [8] are best suited. The suspended geometry largely eliminates the influence of the substrate. A transverse magnetic field B_x is required to create a stable trap while a longitudinal magnetic field B_z suppresses Majorana spin flips [17,18]. With this single-tube setup, neutral atoms in a weak-field seeking state can be trapped. Studying various sources for decoherence, heating or atom loss, and estimating the related time scales, we find that, for reasonable parameters, detrimental effects are small. As a concrete example, we shall consider ^{87}Rb atoms in the weak-field seeking hyperfine state $|F, m_F\rangle = |2, 2\rangle$.

We next describe the setup in Fig. 1, where the (homogeneous) current I flows through the left NT positioned at $(-x_0, 0, z)$. With regard to the decoherence properties of the proposed trap, it is advantageous that the current flows homogeneously through the NT, as disorder effects are usually weak in NTs [8]. Neglecting boundary effects due to the finite tube length L , the magnetic field at $\mathbf{x} = (x, y, z) = (\mathbf{x}_\perp, z)$ is given by

$$\mathbf{B}(\mathbf{x}) = \frac{\mu_0 I}{2\pi} \frac{1}{(x+x_0)^2 + y^2} \begin{pmatrix} -y \\ x+x_0 \\ 0 \end{pmatrix} + \begin{pmatrix} B_x \\ 0 \\ B_z \end{pmatrix} \quad (1)$$

with the vacuum permeability μ_0 . To create a trapping potential minimum, let us write $B_x = \mu_0 I / (2\pi y_0)$. Then the transverse confinement potential is $V(\mathbf{x}_\perp) = \mu |\mathbf{B}(\mathbf{x})|$, where $\mu = m_F g_F \mu_B$ with the Landé factor g_F and the Bohr magneton μ_B . It has a minimum along the line $(-x_0, y_0, z)$, with the distance between the atom cloud and the wire being y_0 . Under the adiabatic approximation [17], m_F is a constant of motion, and the potential is harmonic very close to the minimum of the trap, i.e., $V(\mathbf{x}) \simeq \mu B_z + \frac{1}{2} m \omega^2 [(x+x_0)^2 + (y-y_0)^2]$, with frequency $\omega = [\mu / (m B_z)]^{1/2} \mu_0 I / (2\pi y_0^2)$ and associated transverse confinement length $l_0 = (\hbar / m \omega)^{1/2} \ll y_0$, where m is the atom mass. The adiabatic approximation is valid as long as $\omega \ll \omega_L$ with the Larmor frequency $\omega_L = \mu B_z / \hbar$. Non-adiabatic Majorana spin flips to a strong-field seeking state generate atom loss [1,18] characterized by the rate $\Gamma_{\text{loss}} \simeq (\pi \omega / 2) \exp(1 - 1/\chi)$, with $\chi = \hbar \omega / (\mu B_z)$ [17]. For convenience, we switch to a dimensionless form of the full potential $V(\mathbf{x}_\perp)$ by measuring energies in units of $\hbar \omega$ and lengths in units of l_0 ,

$$\chi V = \left(1 + \chi \frac{d^2 [(x+x_0)^2 - dy + y^2]^2 + d^4 (x+x_0)^2}{[(x+x_0)^2 + y^2]^2} \right)^{1/2}, \quad (2)$$

which depends only on $d = y_0 / l_0$ and χ . The trap frequency then follows as

$$\omega = \frac{m \chi \mu^2}{\hbar^3} \left(\frac{\mu_0 I}{2\pi d^2} \right)^2. \quad (3)$$

Note that a real trap also requires a longitudinal confining potential with frequency $\omega_z \ll \omega$.

To obtain an estimate for the design of the nanotrap, we choose realistic parameters: $\chi = 0.067$, corresponding to a rate of spin flip transition per oscillation period $\Gamma_{\text{loss}} / \omega \sim 10^{-6}$. Decreasing d increases the trap frequency. However, d cannot be chosen too small, for otherwise the potential is not confining anymore (and the harmonic approximation becomes invalid). Using $V(\infty) = \chi^{-1} (1 + \chi d^2)^{1/2}$ for the potential at $|\mathbf{x}_\perp| \rightarrow \infty$, we now show that for $d \lesssim 5$, the harmonic approximation breaks down. To see this, note that for $d = 10$, the potential provides a confining barrier (in units of the trap frequency ω) of $V(\infty) - V(0, 0, z) = 23.8$, while for $d = 5$, we get only $V(\infty) - V(0, 0, z) = 9.8$. Thus exceedingly small values of d would lead to unwanted thermal atom escape processes out of the trap. To illustrate the feasibility of the proposed trap design, we show in Table 1 several parameter combinations with realistic values for the MWNT current together with the resulting trap parameters. In practice, first the maximum possible current should be applied to the NT, with some initial field B_x . After loading of the trap, the field B_x should be increased, the cloud thereby approaching the wire with a steepening of the confinement. At the same time, y_0 and consequently d decrease. This procedure can be used to load the nanotrap from a larger magnetic trap (ensuring mode matching). For a given current, there is a corresponding lower limit y_{min} for stable values of y_0 from the requirement $d \gtrsim 5$, as already mentioned above. To give an example, the confining potential is shown in Fig. 2a) for $I = 100 \mu\text{A}$, representing a reasonable current through thick NTs [8], $d = 10$, $x_0 = l_0$ and $\Gamma_{\text{loss}} / \omega = 10^{-6}$ (where $\chi = 0.067$). The resulting trap frequency is $\omega = 2\pi \times 4.6 \text{ kHz}$ and the associated transverse magnetic field is $B_x = 0.14 \text{ G}$.

3 Influence of destructive effects

For stable operation, it is essential that destructive effects like atom loss, heating or decoherence are small.

(i) One loss process is generated by non-adiabatic Majorana spin flips as discussed above.

(ii) Atom loss may also originate from noise-induced spin flips, where current fluctuations cause a fluctuating magnetic field generating the Majorana spin flip rate [4]

$$\gamma_{\text{sf}} \simeq \left(\frac{\mu_0 \mu}{2\pi \hbar y_0} \right)^2 \frac{S_I(\omega_L)}{2}, \quad S_I(\omega) = \int dt e^{-i\omega t} \langle I(t) I(0) \rangle. \quad (4)$$

At room temperature and for typical voltages $V_0 \approx 1 \text{ V}$, we have $\hbar \omega_L \ll k_B T \ll e V_0$, and $S_I(\omega_L)$ is expected

to equal the shot noise $2eI/3$ of a diffusive wire. For the parameters above, a rather small escape rate results, $\gamma_{\text{sf}} \approx 0.051$ Hz. If a (proximity-induced) supercurrent is applied to the MWNT, the resulting current fluctuations could be reduced even further.

(iii) Thermal NT vibrations might create decoherence and heating, and could even cause a transition to the first excited state of the trap. Using a standard elasticity model for a doubly clamped wire in the limit of small deflections, the maximum mean square displacement is [19]

$$\sigma^2 = \langle \phi^2(L/2) \rangle = k_B T L^3 / (192 Y M_I),$$

where $\phi(z)$ is the NT displacement, L the (suspended) NT length, T the temperature, Y the Young modulus, and M_I the NT's moment of inertia. For $L = 10\mu\text{m}$ and typical material parameters from Ref. [8], we find $\sigma \approx 0.2$ nm at room temperature. This is much smaller than the transverse size l_0 of the atomic cloud. Small fluctuations of the trap center could cause transitions to excited transverse trap states. Detailed analysis shows that the related decoherence rate is also negligible, since the transverse fundamental vibration mode of the NT has the frequency

$$\omega_f = \frac{\beta_1^2}{L^2} \sqrt{\frac{Y M_I}{\rho_L A_c}}, \quad (5)$$

with $\beta_1 \simeq 4.73$, the mass density ρ_L , and the cross-sectional area A_c . For the above parameters, $\omega_f = 2\pi \times 11.9$ MHz is much larger than the trap frequency itself. Due to the strong frequency mismatch, the coupling of the atom gas to the NT vibrations is therefore negligible.

(iv) Another decoherence mechanism comes from current fluctuations in the NTs. Following the analysis of Ref. [6], the corresponding decoherence rate is

$$\frac{\gamma_c}{\omega} = \frac{3\pi}{4\hbar} k_B T \frac{\sigma_0 A}{y_0^3} \left(\frac{\mu_0 \mu_B}{2\pi} \right)^2 \frac{\chi}{\hbar\omega}, \quad (6)$$

where σ_0 is the NT conductivity and A the cross-sectional area through which the current runs in the NT. For the corresponding parameters we find $\gamma_c/\omega < 10^{-8}$.

(v) Another potential source of atom loss could be the attractive Casimir-Polder force between the atoms and the NT surface. The Casimir-Polder interaction potential between an infinite plane and a neutral atom is given by $V_{\text{CP}} = -C_4/r^4$ [5,20]. For a metallic surface and ^{87}Rb atoms, $C_4 = 1.8 \times 10^{-55}$ Jm⁴, implying that at a distance of $1\mu\text{m}$ from the surface, the characteristic frequency associated with the Casimir-Polder interaction is $V_{\text{CP}}/\hbar = 2\pi \times 0.29$ kHz. This represents a fundamental decoherence limit in the kHz regime for conventional on-chip traps with typical current-carrying wire widths $\approx 10\mu\text{m}$. Instead, for our particular design in the nanometer scale, the surface of a NT with a diameter of a few nm covers only a small portion of an infinite plane for distances above 100 nm. Hence, the impact

of the Casimir-Polder interaction should be strongly reduced in our setup. A more detailed estimate, however, goes beyond the scope of this work.

(vi) A further possible mechanism modifying the shape of the confining potential is the influence of the electric field E between the two contacts of the nanowire and the macroscopic leads which is created by the transport voltage V . This field depends strongly on the detailed geometry of the contacts. However, the electric field can in general be reduced if the total length L_{tot} of the NT is increased. (Note that L_{tot} can be different from the length L over which the NT is suspended). Due to the small intrinsic NT resistivity, the influence of the contact resistance then decreases for longer NTs.

4 Number of trapped atoms and size of atom cloud

Next we address the important issue of how many atoms can be loaded in such a nanotrap. This question strongly depends on the underlying many-body physics which determines for instance the density profile of the atom cloud. Since the trap frequencies given in Table 1 exceed typical thermal energies of the cloud, we will consider the 1D situation. Within the framework of two-particle s-wave scattering in a parabolic trap, the effective 1D interaction strength $g_{1\text{D}} = -2\hbar^2/(ma_{1\text{D}})$ is related to the 3D scattering length a according to [12]

$$a_{1\text{D}} = -\frac{l_0^2}{a} \left(1 - \mathcal{C} \frac{a}{\sqrt{2}l_0} \right), \quad (7)$$

where $\mathcal{C} \simeq 1.4603$. Interestingly, $g_{1\text{D}}$ shows a confinement-induced resonance (CIR) for $a = \sqrt{2}l_0/\mathcal{C}$ [12]. For nearly parabolic traps respecting parity symmetry, this CIR is split into three resonances [21]. However, for the typical trap frequencies displayed in Table 1, corresponding to non-resonant atom-atom scattering, the parabolic confinement represents a very good approximation. For free bosons in 1D, the full many-body problem can be solved analytically [22]. It turns out that the governing parameter is given by $n|a_{1\text{D}}|$, where n is the atom density in the cloud. For weak interactions (large $n|a_{1\text{D}}|$), a Thomas-Fermi (TF) gas results, while in the opposite regime, the Tonks-Girardeau (TG) gas is obtained.

For realistic traps with an additional longitudinal confining potential with frequency $\omega_z \ll \omega$, the problem has been addressed in Ref. [23]. The corresponding governing parameter is $\eta = n_{\text{TF}}|a_{1\text{D}}|$ where $n_{\text{TF}} = [(9/64)N^2(m\omega_z\hbar)^2|a_{1\text{D}}|]^{1/3}$ is the cloud density in the center of the trap in the TF approximation. Small η characterizes a TG gas whereas large η corresponds to the TF gas. The longitudinal size ℓ of the atom cloud in terms of the atom number N and the longitudinal (transversal) trap frequencies ω_z (ω) has been computed

in Ref. [23], with the result

$$\ell = \left[\frac{3N(\hbar/m\omega_z)^2}{|a_{1D}|} \right]^{1/3} \quad (8)$$

in the TF regime and

$$\ell = [2N(\hbar/m\omega_z)]^{1/2} \quad (9)$$

in the TG regime. In order to determine the cloud size ℓ , we first calculate η for fixed N, ω_z and ω , and then use the respective formula Eq. (8) or (9). In the crossover region, both expressions yield similar results that also match the full numerical solution [23]. Typical results for realistic parameters are listed in Table 2 for $\omega_z = 2\pi \times 0.1$ kHz. From these results, we conclude that the length of the suspended NT should be in the μm -regime in order to trap a few tens of ^{87}Rb atoms.

To summarize the discussion of the monostable trap, we emphasize that the proposed nanotrap is realistic, with currents of a few 100 μA and lengths of few μm of the suspended parts of NT. No serious decoherence, heating or loss mechanisms are expected for reasonable parameters of this nanotrap.

5 Double-well potential with two carbon nanotubes

In order to illustrate the advantages of the miniaturization to the nanoscale, let us consider a setup which allows two stable minima separated by a tunneling barrier. The simplest setup consists of two parallel NTs carrying co-propagating currents I , a (small) longitudinal bias field B_z and a transverse bias field B_x . Such a double-well potential for 1D ultracold atom gases would permit a rich variety of possible applications. Experiments to study Macroscopic Quantum Tunneling and Macroscopic Quantum Coherence phenomena [24] between strongly correlated 1D quantum gases could then be performed. In addition, qubits forming the building blocks for a quantum information processor could be realized. The rich tunability of the potential shape, including tuning the height of the potential barrier as well as the tunneling distance, is a particularly promising feature.

To realize this potential, we propose to place a second current-carrying NT at $(+x_0, 0, z)$, where the condition $x_0 > y_0$ guarantees the existence of two minima located at $y_0(\pm\sqrt{x_0^2/y_0^2 - 1}, 1)$. By tuning the transversal magnetic field B_x and the current I , y_0 and thus the location of the minima can be modified. Around these minima, the potential is parabolic with frequency

$$\omega = \left[\frac{\mu^2 \chi}{m\hbar} \left(\frac{\mu_0 I}{2\pi} \right)^2 \frac{1}{y_0^2} \left(\frac{1}{y_0^2} - \frac{1}{x_0^2} \right) \right]^{1/3}. \quad (10)$$

Similar to the considerations above, we obtain the potential in units of $\hbar\omega$, which depends only on $d_x = x_0/l_0$, $d_y = y_0/l_0$ and χ ,

$$\chi V = \left(1 + \frac{\chi d_y^4}{1 - d_y^2/d_x^2} \left\{ \left[\frac{-y}{(x+d_x)^2 + y^2} + \frac{-y}{(x-d_x)^2 + y^2} + \frac{1}{d_y} \right]^2 + \left[\frac{x+d_x}{(x+d_x)^2 + y^2} + \frac{x-d_x}{(x-d_x)^2 + y^2} \right]^2 \right\} \right)^{1/2}. \quad (11)$$

Figure 2b) shows the corresponding bistable potential for the particular case of $\chi = 0.067$, $I = 200\mu\text{A}$, $y_0 = 100$ nm and $x_0 = 200$ nm. The two minima are clearly discerned. To see how the frequency in the single well develops if the current in the second wire is turned on, we introduce the reference frequency ω_0 in the single-well case with a fixed current I and a fixed transverse field B_x , such that $y_0 = x_0/2$. Then we obtain the ratio

$$\frac{\omega}{\omega_0} = \left[\frac{1}{16} \left(\frac{x_0}{y_0} \right)^4 \left(1 - \frac{y_0^2}{x_0^2} \right) \right]^{1/3}. \quad (12)$$

For decreasing B_x and keeping I constant, we find that ω decreases as shown in Fig. 3 (black solid line and left scale), while the distance y_0 of the atom cloud increases. In the limit $x_0 = y_0$, the two minima merge and the potential becomes quartic and monostable, implying that $\omega \rightarrow 0$. For the above parameter set, we find $\omega_0 = 2\pi \times 291$ kHz. Since one could obtain the same ω_0 for a larger current I and a correspondingly larger distance x_0 , one gets the same trap frequency for a fixed ratio of y_0/x_0 . However, d_x and d_y themselves would change and since the parabolic frequency ω is fixed, only the non-linear corrections to the parabolic potential will be modified. This in turn influences the height of the potential barrier and the tunneling rate between the two wells. Next we study the influence of the length scale x_0 on these two quantities.

Taking the full potential into account, we calculate the barrier height and the tunneling rate in WKB approximation. The barrier height D separating the two stable wells,

$$\frac{D}{\hbar\omega} = \chi^{-1} \left(1 + \chi d_y^2 \frac{1 - d_y/d_x}{1 + d_y/d_x} \right)^{1/2} - \chi^{-1}, \quad (13)$$

is shown as a function of y_0/x_0 for two values of I in the inset of Fig. 3. Note that the barrier height is of the order of a few multiples of the energy gap in the wells, implying that the potential is in the deep quantum regime, favoring quantum-mechanical tunneling between the two wells. The corresponding tunneling rate Γ for the

lowest-lying pair of energy eigenstates follows in WKB approximation as

$$\frac{\Gamma}{\omega} = e^{-\int_{x_a}^{x_b} dx \sqrt{2[V(x, d_y) - 1]}}, \quad (14)$$

where $x_{a/b}$ are the (dimensionless) classical turning points in the inverted potential at energy $E = \hbar\omega$, which is approximately the ground-state energy of a single well. The integral in Eq. (14) is calculated along the line connecting the two minima corresponding to $y = y_0$. Results for Γ are shown in Fig. 3 (red solid lines and right scale) as a function of y_0/x_0 for two different values of the current I and the distance x_0 yielding the same ω_0 . Note that for the smaller current, $I = 200 \mu\text{A}$, Γ assumes large values already for large frequencies ω . This also implies that the detrimental effects discussed above are less efficient. On the other hand, for large currents, the tunneling regime is entered only for much smaller trap frequencies. For the above parameters, we find $\omega_0 = 2\pi \times 291 \text{ kHz}$. For the smaller current, the tunneling regime starts at frequencies of around $\omega = 0.37\omega_0 = 2\pi \times 108 \text{ kHz}$, corresponding to a temperature of $T = 32 \mu\text{K}$, while for the larger current, the tunneling regime is entered at $\omega = 0.18\omega_0 = 2\pi \times 52 \text{ kHz}$ corresponding to $T = 16 \mu\text{K}$.

A potential drawback of the double wire configuration could be the transverse NT deflection due to their mutual magnetic repulsion. For an estimate, note that the NT displacement field $\phi(z, t)$ obeys the equation of motion $\rho_L \ddot{\phi} = -Y M_I \phi'''' + \mu_0 I^2 / (4\pi x_0)$. The static solution under the boundary conditions $\phi(0, L) = \phi'(0, L) = 0$ is $\phi(z) = \mu_0 [Iz(z-L)]^2 / (96\pi Y M_I x_0)$. Using again parameters from Ref. [8], we find the maximum displacement $\phi(L/2) \approx 0.03 \text{ nm}$ for $L = 10 \mu\text{m}$. Hence the mutual magnetic repulsion of the NTs is very weak. Finally, we note that a potential misalignment of the two NT wires is no serious impediment for the design. Experimentally available techniques could be combined which allow on the one hand to move a NT on a substrate by an atomic force microscope [25], while on the other hand, the NTs can be suspended and contacted after being positioned [26].

6 Conclusions

To conclude, we propose a nanoscale waveguide for ultracold atoms based on doubly clamped suspended nanotubes. All common sources of imperfection can be made sufficiently small to enable stable operation of the setup. Two suspended NTs can be combined to create a bistable potential in the deep quantum regime. When compared to conventional atom-chip traps employed in present experiments, such nanotraps offer several new and exciting perspectives that hopefully motivate experimentalists to realize this proposal.

First, higher trap frequencies can be achieved while at the same time using smaller wire currents. This becomes possible here because both the spatial size of the

atom cloud and its distance to the current-carrying wire(s) would be reduced to the nanometer scale, and because NTs allow typical current densities of $10 \mu\text{A}/\text{nm}^2$, which should be compared to the corresponding densities of $10 \text{ nA}/\text{nm}^2$ in noble metals. For the case of a single-well trap, the resulting trap frequencies go beyond standard chip traps [1]. Large trap frequencies at low currents are generally desirable, since detrimental effects like decoherence, Majorana spin flips, or atom loss will then be significantly reduced.

Second, regarding our proposal of a bistable potential with strong tunneling, the miniaturization towards the nanoscale represents a novel opportunity to study coherent and incoherent tunneling of a macroscopic number of cold atoms. The proposed bistable nanotrap is characterized by considerably reduced tunneling distances, thus allowing for large tunneling rates at large trap frequencies. Note that the energy scale associated with tunneling is larger than thermal energies for realistic temperatures. Such a bistable device could then switch between the two stable states on very short time scales. Within our proposal the parameters of the bistable potential can be tuned over a wide range by modifying experimentally accessible quantities like the current or magnetic fields.

A third advantage of this proposal results from the homogeneity of the currents flowing through the NTs. As NTs are characterized by long mean free paths, they often constitute (quasi-)ballistic conductors, where extremely large yet homogeneous current densities are possible. This distinguishes NTs from the conventionally used wires and could allow to overcome the fragmentation problem [1]. Fragmentation of the atom cloud is presently one of the main impediments to progress in the field of atom-chip traps.

Detection certainly constitutes an experimental challenge in this truly 1D limit. However, we note that single-atom detection schemes are currently being developed, which would also allow to probe the tight 1D cloud here, e.g., by combining cavity quantum electrodynamics with chip technology [2], or by using additional perpendicular wires/tubes ‘partitioning’ the atom cloud [27]. This may then allow to study interesting many-body physics in 1D in an unprecedented manner.

7 Acknowledgments

We thank A. Görlitz, Y. Kobayashi, C. Mora, H. Postma, and J. Schmiedmayer for fruitful discussions. V. P. and M. T. would like to thank H. Takayanagi and K. Semba for the kind hospitality at the NTT Basic Research Laboratories, where parts of this work have been accomplished. We acknowledge support by the German SFB/TR 12 and by the Japanese CREST/JST.

References

1. R. Folman, P. Krüger, J. Schmiedmayer, J. Denschlag, and C. Henkel, *Adv. At. Mol. Opt. Phys.* **48**, 263 (2002)
2. J. Reichel, *Appl. Phys. B* **75**, 469 (2002)
3. H. Ott, J. Fortagh, G. Schlotterbeck, A. Grossmann, and C. Zimmermann, *Phys. Rev. Lett.* **87**, 230401 (2001); W. Hänsel, P. Hommelhoff, T.W. Hänsch, and J. Reichel, *Nature* **413**, 498 (2001); A. Leanhardt, Y. Shin, A. P. Chikkatur, D. Kielpinski, W. Ketterle, and D. E. Pritchard, *Phys. Rev. Lett.* **90**, 100404 (2003); S. Schneider, A. Kasper, Ch. vom Hagen, M. Bartenstein, B. Engeser, T. Schumm, I. Bar-Joseph, R. Folman, L. Feenstra, and J. Schmiedmayer, *Phys. Rev. A* **67**, 023612 (2003)
4. C. Henkel, S. Pötting, and M. Wilkens, *Appl. Phys. B* **69**, 379 (1999)
5. Yu-ju Lin, I. Teper, C. Chin, and V. Vuletić, *Phys. Rev. Lett.* **92**, 050404 (2004)
6. C. Schroll, W. Belzig, and C. Bruder, *Phys. Rev. A* **68**, 043618 (2003)
7. M.A. Kasevich, *Science* **298**, 136 (2002)
8. M.S. Dresselhaus, G. Dresselhaus, and Ph. Avouris (eds.), *Carbon Nanotubes* (Berlin, Springer 2001)
9. D.S. Petrov, D.M. Gangardt, and G.V. Shlyapnikov, *J. Phys. IV France* **116**, 5 (2004)
10. S. Chen and R. Egger, *Phys. Rev. A* **68**, 063605 (2003).
11. I.V. Tokatly, *Phys. Rev. Lett.* **93**, 090405 (2004); J.N. Fuchs, A. Recati, and W. Zwerger, *ibid.* **93**, 090408 (2004); C. Mora, R. Egger, A.O. Gogolin, and A. Komnik, *ibid.* **93**, 170403 (2004)
12. M. Olshanii, *Phys. Rev. Lett.* **81**, 938 (1998); T. Bergeman, M.G. Moore, and M. Olshanii, *ibid.* **91**, 163201 (2003)
13. T. Stöferle, H. Moritz, C. Schori, M. Köhl, and T. Esslinger, *Phys. Rev. Lett.* **92**, 130403 (2004)
14. B. Paredes, A. Widera, V. Murg, O. Mandel, S. Fölling, I. Cirac, G. V. Shlyapnikov, T. W. Hnsch, and I. Bloch, *Nature* **429**, 277 (2004)
15. T. Kinoshita, T. Wenger, and D.S. Weiss, *Science* **305**, 112 (2004)
16. A. Görlitz, J. M. Vogels, A. E. Leanhardt, C. Raman, T. L. Gustavson, J. R. Abo-Shaer, A. P. Chikkatur, S. Gupta, S. Inouye, T. Rosenband, and W. Ketterle, *Phys. Rev. Lett.* **87**, 130402 (2001)
17. C.V. Sukumar and D.M. Brink, *Phys. Rev. A* **56**, 2451 (1997)
18. M. P. A. Jones, C. J. Vale, D. Sahagun, B. V. Hall, and E.A. Hinds, *Phys. Rev. Lett.* **91**, 080401 (2003)
19. S. Sapmaz, Ya.M. Blanter, L. Gurevich, and H.S.J. van der Zant, *Phys. Rev. B* **67**, 235414 (2003)
20. H. B. G. Casimir and D. Polder, *Phys. Rev.* **73**, 360 (1948)
21. V. Peano, M. Thorwart, C. Mora, and R. Egger, unpublished results, see also cond-mat/0411517
22. E. H. Lieb, W. Liniger, *Phys. Rev.* **130**, 1616 (1963)
23. V. Dunjko, V. Lorent, and M. Olshanii, *Phys. Rev. Lett.* **86**, 5413 (2001)
24. U. Weiss, *Quantum Dissipative Systems* (World Scientific, Singapore, 1999)
25. H. W. Ch. Postma, A. Sellmeijer, and C. Dekker, *Adv. Mater.* **17**, 1299 (2000)
26. G.-T. Kim, G. Gu, U. Waizman, and S. Roth, *Appl. Phys. Lett.* **80**, 1815 (2002)

Table 1 Trap frequencies ω , distances y_0 of the atomic cloud from the NT wire, and oscillator lengths l_0 for $\chi = 0.067$ and various I, d .

$I(\mu\text{A})$	d	$\omega(\text{kHz})$	$y_0(\text{nm})$	$l_0(\text{nm})$
1000	10	$2\pi \times 460$	144	14
250	5	$2\pi \times 460$	72	14
250	10	$2\pi \times 28.7$	576	58
100	5	$2\pi \times 73.8$	180	36
100	10	$2\pi \times 4.6$	1440	144
50	5	$2\pi \times 18.4$	360	72
25	5	$2\pi \times 4.6$	720	144

Table 2 Typical results for the longitudinal size ℓ of the ^{87}Rb cloud for realistic values of the transversal trap frequency ω and the atom number N , where $\omega_z = 2\pi \times 0.1$ kHz. For η , see text.

$\omega(\text{kHz})$	$a_{1D}(\text{nm})$	N	η	$\ell(\mu\text{m})$
$2\pi \times 460$	-26.65	30	0.11	7.7
$2\pi \times 460$	-26.65	50	0.15	10
$2\pi \times 73.8$	-223	30	0.67	7.3
$2\pi \times 73.8$	-223	50	0.94	8.7
$2\pi \times 73.8$	-223	100	1.49	11
$2\pi \times 28.76$	-603	30	2.55	5.3
$2\pi \times 28.76$	-603	50	3.58	6.3
$2\pi \times 28.76$	-603	100	5.72	7.9

27. J. Reichel and J.H. Thywissen, *J. Phys. IV France* **116**, 265 (2004)

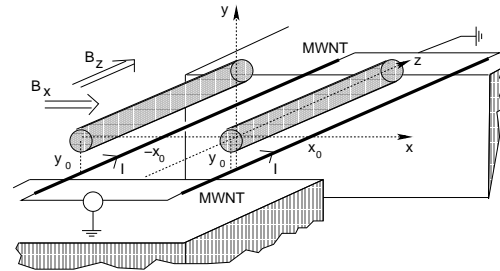


Fig. 1 Sketch of the proposed device. A current-carrying suspended NT is positioned at $(-x_0, 0, z)$ and together with the transverse magnetic field B_x , a 1D trapping potential is formed. The shaded region indicates the atom gas. A similar two-wire setup allows the creation of a bistable potential.

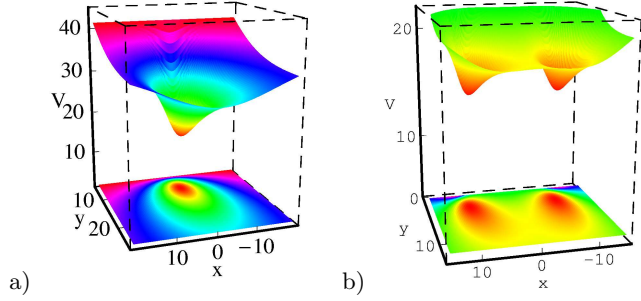


Fig. 2 (Color online). (a) Transverse trapping potential of the nanoscale waveguide for $I = 100 \mu\text{A}$, $d = 10$, $\chi = 0.067$ and $x_0 = l_0$. The resulting trap frequency is $\omega = 2\pi \times 4.6$ kHz while $y_0 = 1440$ nm, corresponding to $B_x = 0.14$ G. (b) Bistable potential for the double-wire configuration for $\chi = 0.067$, $I = 100 \mu\text{A}$, $x_0 = 200$ nm and $y_0 = 100$ nm.

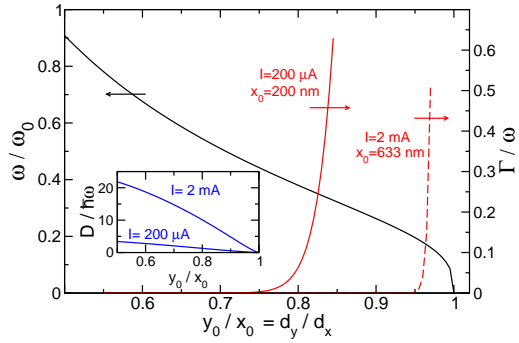


Fig. 3 (Color online). Trap frequency ω in the bistable potential (left scale) and tunneling rate Γ within the WKB-approximation (right scale) as a function of the ratio $y_0/x_0 = d_y/d_x$. For the definition of ω_0 , see text. The tunneling rate Γ is computed for ^{87}Rb atoms with $\chi = 0.067$ and $x_0 = 200$ nm for two values of the current I given in the figure.